PROCEEDINGS OF SCIENCE

Measurement of the RF ice dielectric permittivity & implications for ν reconstruction

T. Jordan (U. Bristol) and U. Latif (U. Kansas, on behalf of ARA) *†

E-mail: uzair.latif@ku.edu

Using radio receiver data triggered by in-ice transmitters, at 0-1.6 km depths at South Pole, we present measurements of the radio-frequency ice dielectric permittivity. Three custom high-amplitude pulsers, with 1–5 ns rise times, were used: a) a piezo-electric pulser, based on the same design previously used for the NASA-sponsored HiCal project in Antarctica, a pulser developed by the KU Instrumentation Design Lab ("IDL"), based on the fast discharge of a DC→DC converter, and the High-Voltage SPark "HVSP" pulser, based on the breakdown of a transistor array. The pulser output is fed into a custom fat-dipole designed to match the geometry of the SPICE core, with one of the dipole chambers hermetically sealed to contain the signal generator and associated power. Signals from the transmitters were recorded on the five englacial multi-receiver ARA stations, as well as ARIANNA Station 51, with receiver depths between 0–200 m, and horizontal baselines of 0.5–5 km. This permits improved measurements of the radio-frequency response of cold, polar ice and also comparison with models of the RF properties of ice crystals, based on direct measurements of the crystal-fabric from SPICE core samples. We find: a) the real part of the permittivity, corresponding to the refractive index, has a depth dependence which can be (at our current level of precision) parameterized as n(z)=1.78-0.43$e^{0.0125z}$, with z in meters and negative with depth, b) from five separate data samples, the field attenuation length, corresponding to the imaginary part of the permittivity is measured to be 1.4–1.8 km in the upper km of the ice sheet, c) the tensorial component of the permittivity, corresponding to birefringence, is measured at a level commensurate with first-principles modeling of the ice fabric, based on core samples extracted during SPICE drilling. Birefringence therefore holds the possibility that the range to an in-ice neutrino interaction can be estimated from the arrival time difference of two polarizations.

36th International Cosmic Ray Conference -ICRC2019-
July 24th - August 1st, 2019
Madison, WI, U.S.A.

*Speaker.
†the ARA Collaboration author list is at http://ara.wipac.wisc.edu/authorlist

PoS(ICRC2019)843

Radio-frequency in-ice Neutrino Detection

The ARA[1], ANITA[2] and ARIANNA[3] experiments seek measurement of ultra-high energy neutrinos via the coherent radio-frequency (RF) Cherenkov radiation produced when a neutrino interacts with cold, polar ice. The smallness of the neutrino interaction cross-section coupled with the small fluxes at high energies demand a large target in order to observe events. The so-called effective volume ($V_{\rm eff}$) defines the equivalent ice volume, as a function of incident neutrino energy over which interactions can be measured.[1] The effective volume is directly dependent on the RF complex ice dielectric permittivity $\vec{\varepsilon} = \varepsilon'(\omega) + \varepsilon''(\omega)$ at 10 MHz–1000 MHz frequencies. The real component ε' determines limitations on $V_{\rm eff}$ from ray-tracing, while the imaginary component limits $V_{\rm eff}$ due to absorption. Both of these are important considerations for detection of neutrinos at very high energies ($E >$1 EeV), although at the low end of the sensitive energy regime (10 PeV), the effective volume is limited not by attenuation or ray tracing, but by the intrinsic signal strength. The "loss tangent", defined as the ratio of the imaginary to the real components of the permittivity ($\tan\delta = \varepsilon''/\varepsilon'$), is related to the attenuation coefficient α by $\alpha = 8.686(2\pi f/c)\sqrt{\varepsilon'}\tan\delta$ and the field attenuation length $L_\alpha = 1/\log\left(10^{\alpha/20}\right)$[4]. The ice response is expected to be relatively flat in the radio regime of hundreds of MHz (the loss tangent is a minimum at $\sim$ 300 GHz [5, 6]), between the two Debye resonances at kHz frequencies and the infra-red peak, and is therefore a suitable frequency region for neutrino detection experiments.

To date, much of our information about the interior of the polar ice sheets has been derived from extensive compilations of radar sounding survey data such as those of BEDMAP [7] or CReSIS [8], in which an airborne transmitter (Tx) beams radio-frequency signal towards the surface from a height of 500 m-1 km, and the returns from the ice below are then recorded. These data have been used to map out ice sheet internal layers and bedrock topography, which can then inform models of ice flow and mass balance. These measurements have been complemented by site-specific mono-static and bi-static radar probes at a variety of locales across the ice sheets.

The South Pole Ice Core Experiment (SPICE)

SPICE proposed to take an ice core sample approximately 3 km from the geographic South Pole, relatively far from the nearest ice divide, allowing a range of novel glaciological studies complementing previous cores taken elsewhere on the Antarctic continent (Byrd Station, Dome C, Vostok, etc.). That core, drilled to 1751 meters, and back-filled with estisol-240 drilling fluid, can also serve as a platform for extensive radioglaciological studies. The ARA (Askaryan Radio Array) and ARIANNA (Antarctic Ross Ice-Shelf ANtenna Neutrino Array) experiments taking data at the South Pole conveniently provide pre-existing, dedicated radio-frequency receiver arrays, over a wide range of receipt angles and horizontal distances, relative to a dedicated transmitter lowered into the 97-mm caliber SPICE icehole. Among the most interesting measurements are signal propagation time delays as a function of polarization (birefringence), as this may allow an estimate of the distance to a putative in-ice source point based on the polarization-dependent arrival time.

[1] Equivalently, some experiments prefer to quote an effective area $A_{\rm eff}$, corresponding to the two-dimensional projection of $V_{\rm eff}$.

In a simple uniaxial model, the signal k-vector is perpendicular to orthogonal ordinary (fast) vs. extraordinary (slow) axes, with $\vec{E}$ projected onto o or e. For oblique incidence, the s-polarization (horizontal) and p-polarization (vertical, at glancing incidence) components comprise the natural polariation basis, and a three-dimensional biaxial propagation model is invoked.

Modelling ice birefringence and oblique radio wave propagation using the SPICE core data

The oblique propagation model is restricted to rotation in the planes of the principal axes of the dieletric tensor. As the signal advances the E-field polarizations project onto the principal axes of the permittivity tensor, resulting in different propagation velocities and a net, distance-dependent, time delay.This double refraction model is equivalent to Fermat's least time principle being satisfied separately by each polarization mode, and is similar to models of oblique propagation in birefringent thin film reflectors (e.g. [9]). The model enables calculation of the s-p time delay for rotation in the planes of the principal axes, which serve as bounding cases for the observed h-v time delays at the receiver stations[10].

Representing the bulk dielectric anisotropy of polar ice At radio frequencies the bulk dielectric tensor and principal refractive indices of polar ice can be modeled from ice fabric measurements (the c-axis orientation distribution) [11]. This effective medium approach was developed to interpret polarimetric radar sounding measurements (e.g. [11, 12, 13]) and assumes that the dimensions of the ice crystal grains ($\sim$ mm) are much less than radio wavelengths. Individual ice Ih crystals have hexagonal structure and are uniaxially birefringent with the optic axis aligned with the crystallographic axis (c-axis) [14]. The magnitude of the crystal birefringence (in terms of the permittivity) is given by $\Delta\varepsilon' = (\varepsilon_{\|c} - \varepsilon_{\perp c})$, where $\varepsilon_{\|c}$ and $\varepsilon_{\perp c}$ are the principal permittivities parallel and perpendicular to the c-axis, and with $\varepsilon_{\|c} > \varepsilon_{\perp c}$ [15]. (The notation $\Delta\varepsilon'$ is used as the radar sounding literature normally uses $\Delta\varepsilon$ for the bulk birefringence.) At radio frequencies ($\sim$ 500 MHz), as ice temperature increases from -60° C to 0° C, $\Delta\varepsilon'$ increases by $\sim$ 5% from $\sim$0.0325-0.0345 [15, 16].

Ice fabric measurements consist of thin ice core sections that measure the ice crystal orientation distribution in terms of a second order ellipsoidal orientation tensor (e.g. [17, 18]), for which the eigenvalues, E_1, E_2, E_3 represent the relative c-axis concentration, projected along each principal coordinate direction. The eigenvalues have the properties $E_1 + E_2 + E_3 = 1$ and, by convention we assume, $E_3 > E_2 > E_1$. Using this eigenvalue framework, the bulk principal dielectric tensor is a diagonal matrix with elements $\varepsilon_i = \varepsilon_{\perp c} + E_i\Delta\varepsilon'$, etc. (see Appendix of [11] for the derivation). For the general case ($E_1 \neq E_2 \neq E_3$), polar ice therefore behaves as a biaxial medium, i.e., three different principal permittivities. The familiar principal refractive indices, which correspond to the axes of the biaxial indicatrix ellipsoid (refer to [19] for more details of this representation) are given by $n_i = \sqrt{\varepsilon_{\perp c} + E_i\Delta\varepsilon'}$.

The stresses present in an ice sheet shape the local ice fabric. Due to ice viscosity being an order of magnitude higher parallel to the c-axis than perpendicular, aggregates of ice crystals tend to align toward the compression (primarily due to the vertical ice overburden) axis and away from the extension axis [20]. End-member classes used to describe ice fabrics are: 'random' ($E_1 \approx E_2 \approx E_3 \approx \frac{1}{3}$ and associated with the near-surface),'single-pole' ($E_1 \approx E_2 \approx 0, E_3 \approx 1$ and associated with

the deepest ice undergoing compression), and an intermediate 'vertical girdle' ($E_1 \approx 0, E_2 \approx E_3 \approx \frac{1}{2}$ and associated with lateral tension). Visual examples of different fabrics are provided in [21].

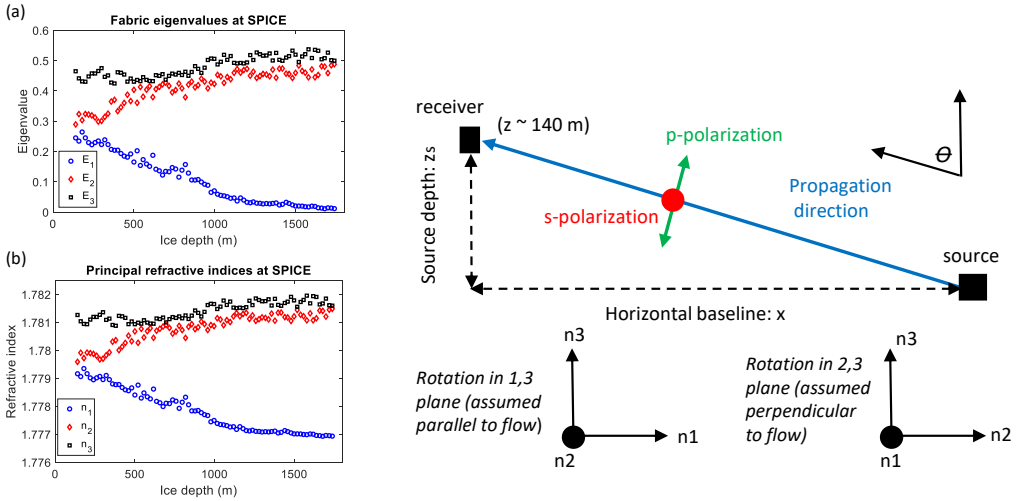

Figure 1: Left: (a) Fabric eigenvalues from the SPICE ice core. (b) Eigenvalues translated into refractive indices. Right: Schematic diagram for oblique propagation model. The model considers rotation in the 1,3 and 2,3 planes; the principal dielectric axes of each layer in relation to the s and p polarizations are indicated.

Principal refractive indices profiles from the SPICE core. Figure 1(a) shows fabric eigenvalue profiles from the SPICE ice core at a $\sim$ 20 m vertical resolution. The plot indicates a development from a relatively random fabric in shallower ice ($E_3 \approx 0.45, E_2 \approx 0.30, E_1 \approx 0.25$ at $z = 150$ m) to a vertical girdle fabric in deeper ice ($E_3 \approx 0.50$, $E_2 \approx 0.49$, $E_1 \approx 0.01$ at $z = 1750$ m). Profiles for the principal refractive indices, calculated as above, with $\varepsilon_{\perp}$=3.157 (corresponding to a polarization-averaged refractive index of $\bar{n} = 1.78$) and $\Delta\varepsilon' = 0.034$, are shown in Fig. 1(b).

Since the azimuthal orientation of the core fabric sections are typically not recorded during drilling, the E_1 and E_2 directions are unknown. Due to the dominance of vertical compression, the E_3 eigenvector (greatest c-axis concentration) is generally close to being aligned with the vertical [19], and is typically approximated as vertical in polarimetric radar sounding studies [11, 13, 22]. For an ice flow model where there is a lateral component of tension present the E_2 eigenvector (greatest c-axis concentration in horizontal plane) is expected to be approximately perpendicular to the horizontal flow direction, with the E_1 eigenvector parallel to flow [11, 18]. Using polarimetric radar sounding, this predicted behavior has been verified at ice divides such as the NEEM ice core region in Northern Greenland [22].

Modelling oblique radio wave propagation and the s-p time delay In the radio propagation model we assume that the ice sheet can be modelled as a stratified anisotropic medium. Each layer of the ice sheet has thickness δz_i which is determined from the vertical spacing of the SPICE core eigenvalue data (generally 20 m). The dielectric properties of each layer are defined by the dielectric tensor (the set of Principal RIS). We assume the canonical fabric orientation described

above, with the E_3 eigenvector vertical, the E_2 eigenvector perpendicular to the ice flow direction, and E_1 eigenvector parallel.

The model considers two rotation scenarios: (i) rotation in the plane of the E_1 and E_3 eigenvectors (assumed perpendicular to flow), (ii) rotation in the plane of the E_2 and E_3 eigenvectors (assumed parallel to flow). A schematic diagram of how this relates to the radio sources and receiver stations in shown in Fig. 1 (right), with the electric field resolved into conventional s and p components (perpendicular and parallel to the rotation/incidence plane). Computationally the model is set-up with source depth and the horizontal baseline fixed, and with $\sin(\theta_{p,0})$ and $\sin(\theta_{s,0})$ (the s-polarization and p-polarization incidence angles at the source layer) as degrees of freedom to be solved for at each step along signal propagation. For rotation in the 1,3 plane, the s and p polarization refractive indices of the i^{th} layer are given by

$$n_{s,i} = n_{2,i}, \tag{1}$$

$$n_{p,i} = \frac{n_{3,i} n_{1,i}}{\sqrt{n_{1,i}^2 \sin^2(\theta_{p,i}) + n_{3,i}^2 \cos^2(\theta_{p,i})}}, \tag{2}$$

where the first subscript indicates the principal refractive index component, and with $\theta_{p,i}$ the p-polarization propagation angle in the i^{th} layer [9, 19]. For rotation in the 2,3 plane the 1 and 2 subscript indices are interchanged in the equations above. The propagation angles in each layer are derived from separate applications of Snells' law: $n_{p,i}\sin(\theta_{p,i}) = n_{p,0}\sin(\theta_{p,0})$, with an analogous s-component expression (refer to [9] for analytical expressions for $(\theta_{p,i})$ in terms of the principal refractive indices).

In each layer of the ice sheet the s/p radio path lengths are given by, e.g., $\delta r_{p,i} = \frac{\delta z_i}{\cos(\theta_{p,i})}$ which corresponds to layer time increments $\delta t_{p,i} = \delta r_{p,i} n_{p,i}/c$. The total s-p time delay is then given by $\Delta T_{s,p} = \sum_i \delta t_{s,i} - \sum_i \delta t_{p,i}$, and $\Delta T_{s,p} < 0$ therefore corresponds to the s polarization arriving at the detector before the p polarization.

Model results Figure 2(a) shows $\Delta T_{s,p}$ as a function of ice depth for horizontal baselines which pair the ARA receiver stations A2 and A4 with the SPICE and so-called 'deep pulser' sources. The corresponding angles of incidence for the A2 receiver station are shown in Fig. 2(b). Figure 2(a) indicates that for rotation in the 2, 3 plane (assumed perpendicular to flow, as is approximately the case for A2), $\Delta T_{s,p} < 0$ and increases with the radio path length, with $\Delta T_{s,p} \sim$ -50 to -20 ns. For rotation in the 1, 3 plane (assumed parallel to flow, as is approximately the case for A4) $\Delta T_{s,p}$ increases with optical path length but is relatively minor ($|\Delta T_{s,p}| < 10$ ns).

There is a simple explanation for the relationships in Fig. 2(a) in terms of the depth profiles for n_s and n_p and the associated birefringence $\Delta_n = n_s - n_p$. For rotation in the 2, 3 plane (assumed perpendicular to flow) n_s is given by n_1 and n_p is given by a mixing of n_2 and n_3, Fig. 2(c). In this case the birefringence is significant; corresponding to a depth-averaged fractional value $|n_s - n_p|/\bar{n}$ $\sim 0.11\%$ at 55° and $\sim 0.16\%$ at 80°. Additionally $n_s - n_p < 0$ holds for all incidence angles/source depths, and therefore $\Delta T_{s,p} < 0$.

For rotation in the 1, 3 plane (assumed parallel to flow), n_s is given by n_2 and n_p is given by a mixing of n_1 and n_3, as shown in Fig. 2(d). In this case the birefringence is relatively minor; corresponding to a depth-averaged fractional value of $|n_s - n_p|/\bar{n} \sim 0.04\%$ at 55° and $\sim 0.03\%$ at 80°. The sign for $n_s - n_p$ also switches from positive to negative as the angle of incidence increases

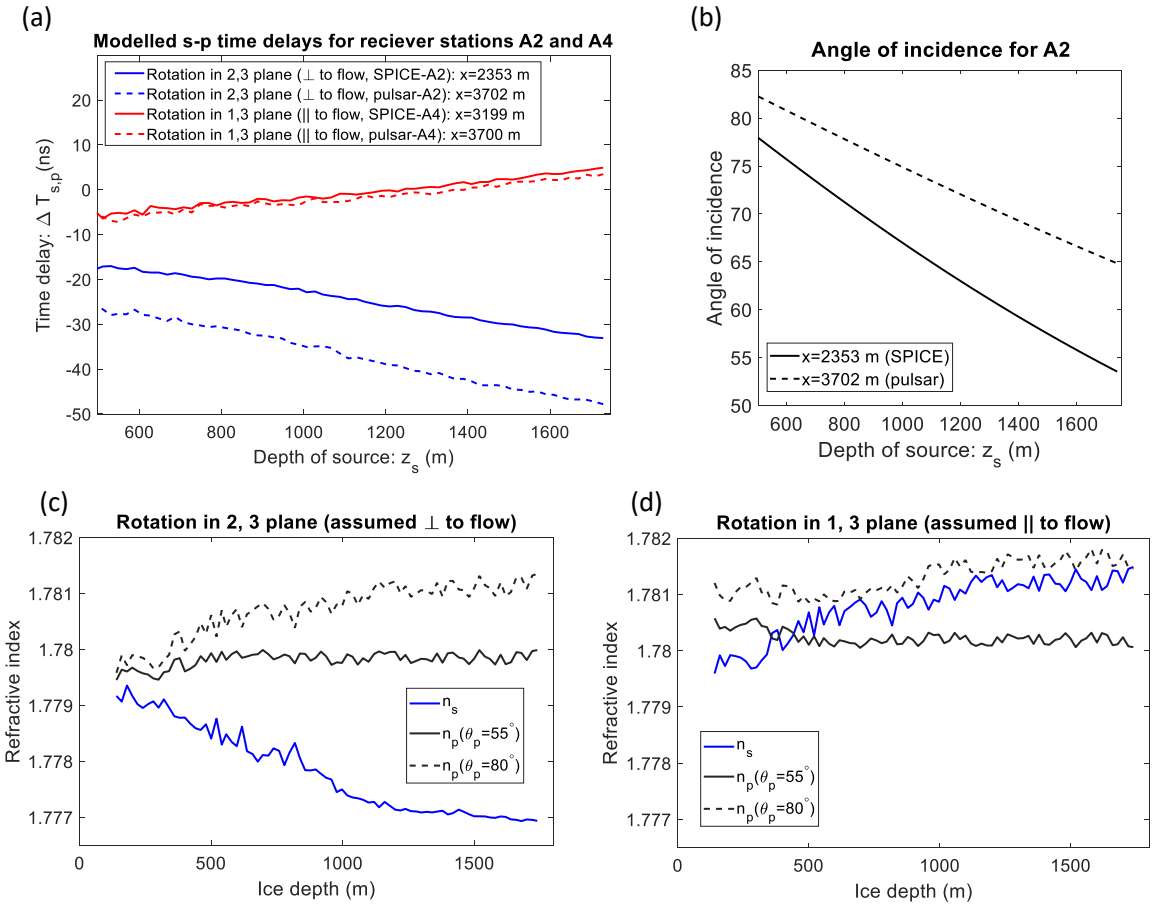

Figure 2: (a) s-p time delays for horizontal baseline geometries roughly corresponding to the A2 and A4 receiver stations. (b) Angle of incidence as a function of ice depth for the A2 receiver station. (c) n_s and n_p for rotation perpendicular to flow. (d) n_s and n_p for rotation parallel to flow.

(source depth decreases). This result also explains why there is a shift in the sign of $\Delta T_{s,p}$ from negative to positive as the source depth increases in Figure 2(a). The experimental value for A4 is $\Delta T_{H,V} = 2 \pm 4$ ns.

The values of $\Delta T_{s,p}$ for rotation in the 2, 3 plane (perpendicular to flow) can be compared with the measured h-v time delays for the A2 receiver station (angle to flow $\sim 64\,^{\circ}$, $z_s \sim 1000$ m for the SPICE source; angle to flow $\sim 78\,^{\circ}$, $z_s \sim 1400$ m for the pulser source). For the SPICE source the measured h-v time delay is $\sim$ -16 ns (approximate mean value) and the modeled s-p time delay is -23 ns. For the deep-pulser source the measured h-v time delay is $\sim$ -27 ns (approximate mean value) and the modeled s-p time delay is -43 ns. The magnitude of the modeled time delays are therefore greater than measured by $\sim$ 30-40%.

The overestimate of the modeled time delay magnitude is unsurprising, as the model (formulated for a propagation angle in the planes of the principal axis system) represents a bounding case where the refractive index contrast and birefringence is greatest. A more general propagation model

(formulated for a general propagation direction relative to the principal axis system) would result in wave-splitting and a coupling of the polarization modes, and is currently under development.

Model/Experiment discrepancies As noted above, despite it's simplicity, the forward modelling of ice bulk birefringence using fabric data, and constructing a bounding proportion model for polarization time delays presented herein, provides relatively good agreement with the ARA data. However, it should be noted that the model does not agree as well with older RICE bedrock-reflection data[23], for which transmitter and receiver were separated horizontally by approximately 25 meters, and December, 2018 ARIANNA Spice Core data. In contrast to the predominantly horizontal propagation of signals from the Spice Core to ARA, the launch angles are $\mathcal{O}$(1–10) degrees off vertical for those RICE and ARIANNA data sets, respectively.

Summary and Plans for 2019-2020

As illustrated herein, the SPICE core represents a tremendous resource for making glaciological measurements. In addition to the data taken in 2018-19, there are three other obvious objectives for additional future work – first, one would like to map out the frequency dependence of the attenuation length using an in-ice continuous wave (CW) signal generator; second, one would like to map out so-called 'shadow zone' propagation along ray trajectories classically forbidden for media with uniformly-varying refractive index dependence on depth; finally, one would like to probe the dielectric constant using a primarily HPol-broadcasting antenna. The first two of these will be studied using SPICE core data to be taken in December, 2019–January, 2020. The third of these will require a new, dedicated transmitter antenna, currently under development at the University of Kansas and part of a transmitter R&D program designed to operate in concert with a radio component of the Gen-2 Project.

References

[1] Patrick Allison, Jan Auffenberg, Robert Bard, JJ Beatty, DZ Besson, Sybille Böser, C Chen, Pisin Chen, Amy Connolly, Jonathan Davies, et al. Design and initial performance of the askaryan radio array prototype eev neutrino detector at the south pole. *Astroparticle Physics*, 35(7):457–477, 2012.

[2] PW Gorham, P Allison, SW Barwick, JJ Beatty, DZ Besson, WR Binns, C Chen, P Chen, JM Clem, A Connolly, et al. The antarctic impulsive transient antenna ultra-high energy neutrino detector: Design, performance, and sensitivity for the 2006–2007 balloon flight. *Astroparticle Physics*, 32(1):10–41, 2009.

[3] SW Barwick, EC Berg, DZ Besson, G Binder, WR Binns, David J Boersma, RG Bose, DL Braun, JH Buckley, V Bugaev, et al. A first search for cosmogenic neutrinos with the arianna hexagonal radio array. *Astroparticle Physics*, 70:12–26, 2015.

[4] C. R. Bentley V. V. Bogorodsky and P. E. Gudmansen. *Radioglaciology*, volume 1 of *1*. Reidel, P.O. Box 17, 3300 AA Dordrecht, Holland, 1 edition, 1 1985.

[5] Stephen G Warren. Optical constants of ice from the ultraviolet to the microwave. *Applied optics*, 23(8):1206–1225, 1984.

[6] Stephen G Warren and Richard E Brandt. Optical constants of ice from the ultraviolet to the microwave: A revised compilation. *Journal of Geophysical Research: Atmospheres*, 113(D14), 2008.

[7] P Fretwell, Hamish D Pritchard, David G Vaughan, JL Bamber, NE Barrand, R Bell, C Bianchi, RG Bingham, DD Blankenship, G Casassa, et al. Bedmap2: improved ice bed, surface and thickness datasets for antarctica. *The Cryosphere*, 7(1), 2013.

[8] B. Panzer et al. An ultra-wideband, microwave radar for measuring snow thickness on sea ice and mapping near-surface internal layers in polar firn. *J. Glac.*, 59(214):375–393, 1 2013.

[9] S. J. Orfanidis. Electromagnetic waves and antennas: Chapter 8, 2016.

[10] Michael F Weber, Carl A Stover, Larry R Gilbert, Timothy J Nevitt, and Andrew J Ouderkirk. Giant birefringent optics in multilayer polymer mirrors. *Science*, 287(5462):2451–2456, 2000.

[11] Shuji Fujita, Hideo Maeno, and Kenichi Matsuoka. Radio-wave depolarization and scattering within ice sheets: a matrix-based model to link radar and ice-core measurements and its application. *Journal of Glaciology*, 52(178):407–424, 2006.

[12] Kenichi Matsuoka, Donovan Power, Shuji Fujita, and Charles F. Raymond. Rapid development of anisotropic ice-crystal-alignment fabrics inferred from englacial radar polarimetry, central West Antarctica. *Journal of Geophysical Research: Earth Surface*, 117(3):1–16, 2012.

[13] A. M. Brisbourne, C. Martin, A .M. Smith, A. F. Baird, J. M. Kendall, and J Kingslake. Constraining Recent Ice Flow History at Korff Ice Rise, West Antarctica, Using Radar and Seismic Measurements of Ice Fabric. *Journal of Geophysical Research: Earth Surface*, 124:175–194–373, 2019.

[14] N. D. Hargreaves. The radio-frequency birefringence of polar ice. *Journal of Glaciology*, 21(85):301–313, 1978.

[15] S Fujita, T Matsuoka, T Ishida, K Matsuoka, and S Mae. A summary of the complex dielectric permittivity of ice in the megahertz range and its applications for radar sounding of polar ice sheets. *Physics of Ice Core Records*, 104:185–212, 2000.

[16] T Matsuoka, S Fujita, and S Mae. Effect of temperature on dielectric properties of ice in the range 5−39 ghz. *Journal of Applied Physics*, 80(109), 1996.

[17] M Montagnat, N Azuma, J Eichler, S Fujita, S Kipfstuhl, and D Samyn. Fabric along the NEEM ice core, Greenland, and its comparison with GRIP and NGRIP ice cores. *The Cryosphere*, 8:1129–1138, 2014.

[18] Y Wang, T Thorsteinsson, J Kipfstuhl, H Miller, D Dahl-Jensen, and H Shoji. A vertical girdle fabric in the NorthGRIP deep ice core. *Journal of Glaciology*, 35:515–520, 2002.

[19] K. Matsuoka, L. Wilen, S.P. Hurley, and C.F. Raymond. Effects of Birefringence Within Ice Sheets on Obliquely Propagating Radio Waves. *IEEE Transactions on Geoscience and Remote Sensing*, 47(5):1429–1443, may 2009.

[20] Richard B Alley. Fabrics in polar ice sheets: Development and prediction. *Science*, 240(4851):493–495, 1988.

[21] N.H. Woodcock. Specification of fabric shapes using an eigenvalue method. *Geological Society of America Bulletin*, 88:1231–1236, 1977.

[22] T. M. Jordan, D. M. Schroeder, D. Castelletti, J. Li, and J. Dall. A Polarimetric Coherence Method to Determine Ice Crystal Orientation Fabric From Radar Sounding: Application to the NEEM Ice Core Region. *IEEE Transactions on Geoscience and Remote Sensing*, 2019.

[23] I Kravchenko, D Besson, Andres Ramos, and Juliet Remmers. Radio frequency birefringence in south polar ice and implications for neutrino reconstruction. *Astroparticle Physics*, 34(10):755–768, 2011.